THE JOURNAL OF PHYSICAL CHEMISTRY B

Article

Cite This: J. Phys. Chem. B 2019, 123, 1672−1678

pubs.acs.org/JPCB

Temperature Dependence of Static Structure Factor Peak Intensities for a Pyrrolidinium-Based Ionic Liquid

Travis Mackoy,[†] Nicholas A. Mauro,[‡] and Ralph A. Wheeler*[,†]

[†]Department of Chemistry and Biochemistry, Northern Illinois University, DeKalb, Illinois 60115, United States

[‡]Department of Physics, St. Norbert College, De Pere, Wisconsin 54115, United States

Supporting Information

ABSTRACT: Static structure factors ($S(q)$) for many ionic liquids show low-wavenumber peaks whose intensities increase with increasing temperature. The greater peak intensities might seem to imply increasing intermediate-range order with increasing temperature. Molecular dynamics (MD) simulations for a representative ionic liquid, 1-butyl-1-methylpyrrolidinium bis(trifluoromethylsulfonyl)imide (C_4C_1pyrrTFSI), were used to calculate $S(q)$ and partial $S(q)$ (cation−cation, anion−anion, and cation−anion) at 298, 363, and 500 K. $S(q)$ and partial $S(q)$ were further decomposed into positive and negative components (which each indicate structural ordering) by separately summing positive and negative Fourier transform summands. Increasing temperature causes the negative components of each partial $S(q)$ to decrease in magnitude more than the positive components, causing the total $S(q)$ to increase in magnitude. Thus, structural ordering with periodicities corresponding to observed peaks in $S(q)$ does not increase but instead decoheres with increasing temperature, even though $S(q)$ peak heights increase. Fourier transform summands also show where in real space the positive and negative component contributions to $S(q)$ change when the temperature increases. This new, detailed analysis based on Fourier transform summands comprising $S(q)$ argues for great caution when interpreting $S(q)$ intensities and highlights the value of simulations as a complement to X-ray (or neutron) scattering experiments.

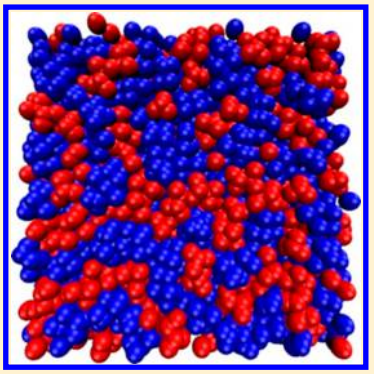

INTRODUCTION

Room temperature ionic liquids (RTILs) are a class of salts which are liquid near ambient temperatures and have potential applications as reaction solvents,[1−3] catalysts,[4,5] sensors,[6] and battery electrolytes.[7] RTILs often have low volatility, low flammability, high thermal stability, and desirable electrochemical windows, making them potential replacements for traditional battery electrolytes, which are often volatile and flammable.[8] While relatively high viscosity is a common drawback, it may be possible to design RTILs (e.g., through tailoring of chemical groups, or varying ion mixtures) that maintain desirable properties and exhibit moderate viscosity. Molecular level insight regarding RTIL structure (e.g., cation−anion ordering) would contribute to understanding of the above properties and aid in tailoring RTILs to suit specific applications.[9,10] Intermediate-range liquid ordering is a signature of many RTILs and manifests as static structure factor ($S(q)$) peaks in the low-wavenumber regime (i.e., $q < 2$ Å^{-1}).[11−14] RTIL intermediate-range ordering is affected by chemical structures and can be modified by, for example, varying alkyl side chain length.[15−23] The RTIL family 1-alkyl-1-methylpyrrolidinium cation with bis(trifluoromethylsulfonyl)-imide anion ($C_nC_1$pyrrTFSI) has been studied experimentally and computationally,[22,24−47] and the $n = 4$ member (C_4C_1pyrrTFSI) is the focus here. $S(q)$ derived from X-ray scattering and MD simulations, including temperature-dependent trends for the two prominent low-q peaks, have been reported for C_4C_1pyrrTFSI.[24−28,30,45] Peak 1 (centered near $q = 0.8$ Å^{-1}) is usually attributed predominantly to charge alternation (i.e., periodic anion−anion and cation−cation ordering at characteristic distances), while peak 2 (centered near $q = 1.25$ Å^{-1}) is usually attributed primarily to charge adjacency (corresponding to near neighbor ions).[24,25] While the shift of these C_4C_1pyrrTFSI peaks to lower q is generally attributed to lower density, their increasing intensity with increasing temperature has been the subject of discussion.[24,25] For phosphonium-based RTILs, increasing peak heights have been attributed to disordering of the apolar, hydrophobic region that allows the polar region to become more ordered.[48] In this work, we find that a decoherence of structural ordering on multiple length scales (with periodicities indicated by values of q where peaks appear in $S(q)$) occurs for C_4C_1pyrrTFSI with increasing temperature.

MD simulations complement X-ray or neutron scattering experiments by allowing assignment of peaks to various ordering, such as charge alternation in RTILs, via decomposition of $S(q)$ into partial $S(q)$.[49,50] Total $S(q)$ can be calculated using eq 1, which is derived from the formalism proposed by Faber and Ziman[51]

Received: January 16, 2019
Revised: January 22, 2019
Published: January 23, 2019

DOI: 10.1021/acs.jpcb.9b00449
J. Phys. Chem. B 2019, 123, 1672−1678

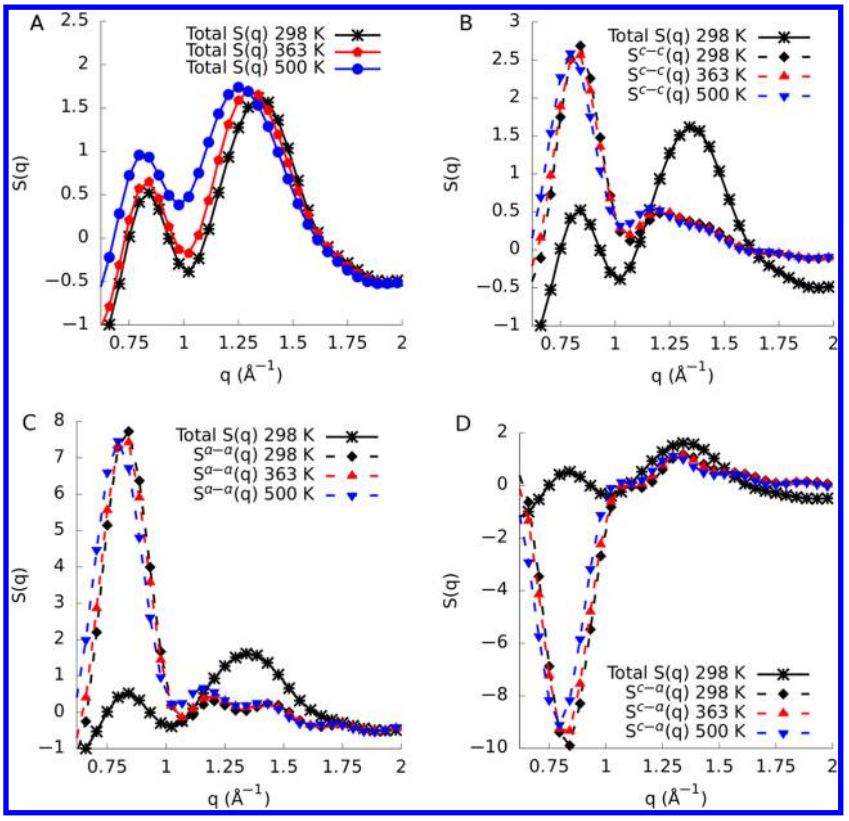

Figure 1. (A) Static structure factor ($S(q)$) showing two low-wavenumber peaks for the ionic liquid 1-butyl-1-methylpyrrolidinium bis(trifluoromethylsulfonyl)imide (C_4C_1pyrrTFSI). The peaks shift to smaller q and increase their intensities with increasing temperature. The left peak (peak 1) corresponds primarily to charge alternation, and the right peak (peak 2) corresponds significantly to charge adjacency. Temperature trends for partial $S(q)$ for cation−cation (B), anion−anion (C), and cation−anion (D) are shown alongside $S(q)$ at 298 K.

$$S(q) = \sum_{i}^{n}\sum_{j}^{n}\sum_{r=0}^{r_{max}} \frac{4\pi\rho_0\chi_{ij}f_i(q)f_j(q)r^2(g_{ij}(r) - 1)\frac{\sin(qr)}{qr}\Delta r}{\left[\sum_i^n \sqrt{\chi_{ii}}f_i(q)\right]^2} \quad (1)$$

where i and j are atom types, n is the number of atom types, $g_{ij}(r)$ is a partial radial distribution function, r_{max} is the maximum distance used to calculate $g_{ij}(r)$, χ_{ij} is the fraction of atomic distances of type i with j within the cutoff r_{max}, $f_i(q)$ is the atomic form factor of i (approximated using a sum of Gaussians[52]), and ρ_0 is the average number density of the system. Partial $S(q)$ are calculated by summing over a restricted range of atom types i and j in eq 1, selected for their chemical significance (e.g., cation−cation).[25−27] The sum from zero to r_{max} represents a discrete Fourier transform, and the summands will be referred to as Fourier transform summands.

The Margulis group provided a physical interpretation of positive and negative partial $S(q)$ calculated at the same q, attributing them to periodic ordering of ions with the same spatial frequency (i.e., q) but offset by a phase shift.[26] The phase shift corresponds to a real space shift of the periodic ordering in the radial distribution function ($g(r)$). When the phase shift is present, the $S(q)$ intensity at a given q becomes negative. They labeled the phase-shifted, negative partial $S(q)$ "anti-peaks".[26] Both peaks and anti-peaks in partial $S(q)$ therefore indicate the presence of ordering. On the basis of their analysis of peaks and anti-peaks, Margulis et al. proposed an explanation for the intensity increase observed for two low-q peaks with increasing temperature for phosphonium-based RTILs.[48]

Here, we extend previously published work by using Fourier transform summands to decompose $S(q)$ and partial $S(q)$ (whether positive or negative) into positive and negative components. This is achieved by separately summing the positive and negative Fourier transform summands for partial $S(q)$. At a given q, the positive and negative components each indicate ordering of a given type (e.g., cation−cation), offset by a real space phase shift. Positive and negative components at a given q have a spatial periodicity characteristic of the cardinal sine function associated with that q, $\mathrm{sinc}(qr) = \sin(qr)/(qr)$. Therefore, plots of positive and negative components offer complementary information to plots of $S(q)$ and partial $S(q)$, irrespective of whether $S(q)$ or partial $S(q)$ are themselves positive or negative.

COMPUTATIONAL DETAILS

Simulation boxes of 250 ion pairs were used for all reported analyses. Simulation boxes of 500 ion pairs did not significantly affect results (not shown). LAMMPS[53] and the CL&P force field[54,55] were used for all simulations. Coulombic and van der Waals cutoffs were 15 Å, and long-range electrostatics was treated using a particle−particle particle−mesh solver[56] with a 10^{-7} desired relative error in forces. Temperature and pressure (1 atm) were controlled using a Nosé−Hoover thermostat (T_{damp} = 100) and barostat (P_{damp} = 500).[57,58] Thermalization at 650 K was performed for 10 ns in order to move molecules away from the initial configuration, which was generated using Packmol.[59] Simulations were then cooled by evenly ramping

DOI: 10.1021/acs.jpcb.9b00449
J. Phys. Chem. B 2019, 123, 1672−1678

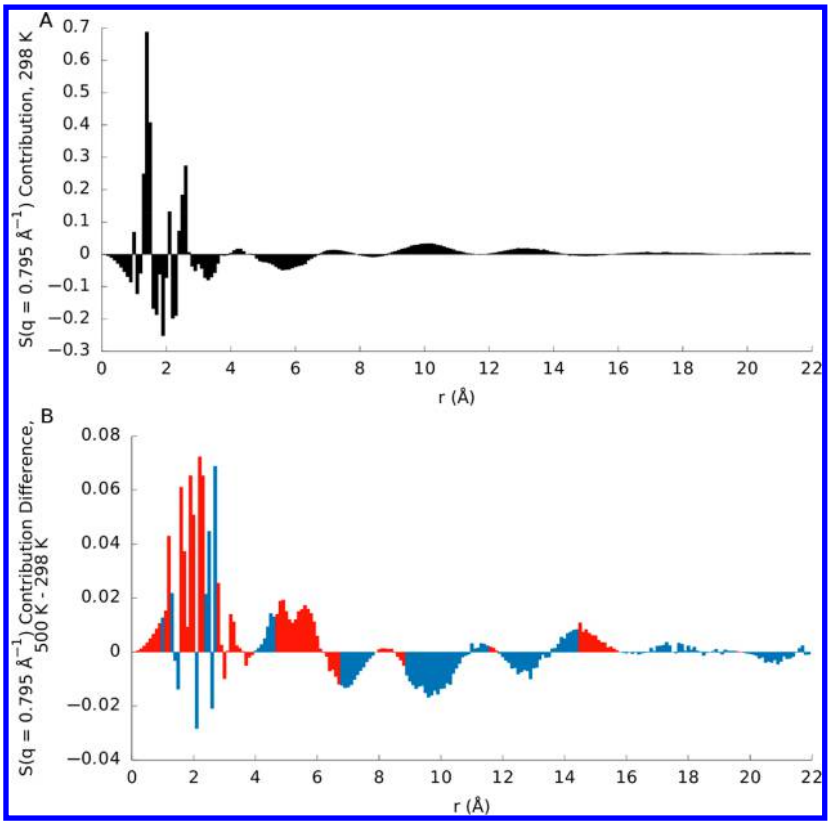

Figure 2. (A) Fourier transform summands for q = 0.795 Å^{-1} at 298 K and (B) differences between 500 and 298 K Fourier transform summands for q = 0.795 Å^{-1}. Fourier transform summands indicate how positive or negative each radial distribution function bin's contribution is to the static structure factor ($S(q)$) at a given q. Summing all Fourier transform summands (in A) gives $S(q)$ at q = 0.795 Å^{-1}. This is identical to solving eq 1 for q = 0.795 Å^{-1}. Summing only the positive or negative Fourier transform summands in A gives the positive or negative component of $S(q)$, respectively. The difference between Fourier transform summands at two temperatures at a given q (e.g., in B) shows where in real space the $S(q)$ contributions became more positive and negative. Differences are colored by whether the summand at 298 K (from A) was positive (blue) or negative (red). Summing all difference terms yields the difference in $S(q)$ at q = 0.795 Å^{-1} between 500 and 298 K.

Table 1. Positive and Negative Components of $S(q)$ and Partial $S(q)$ at q = 0.795 Å^{-1} [a]

	298 K	500 K	difference	percent of difference
$S(q)$	0.42	0.96	0.54	100.00
positive contribution	12.77	12.13	−0.64	−118.47
negative contribution	−12.36	−11.18	1.18	218.47
positive contribution cation−cation	2.99	2.93	−0.06	−10.84
negative contribution cation−cation	−0.48	−0.34	0.14	26.14
positive contribution anion−anion	9.46	9.14	−0.32	−58.97
negative contribution anion−anion	−2.17	−1.68	0.49	90.61
positive contribution cation−anion	0.32	0.06	−0.26	−48.66
negative contribution cation−anion	−9.71	−9.16	0.55	101.71

[a]Positive and negative contributions to $S(q)$ (rows 2 and 3) each indicate structural ordering and sum to $S(q)$ (row 1). Positive and negative contributions to partial $S(q)$ (rows 4−9) also sum to $S(q)$ (row 1). For increasing temperature (298 to 500 K), the negative contribution decreases in magnitude more than the positive contribution, which causes $S(q)$ to increase in magnitude with increasing temperature. Numbers are rounded to two decimal places.

the temperature from 650 K to the final temperatures over 10 ns. Next, 100 ns of equilibration simulation was performed at each final temperature, followed by 10 ns of production simulation (storage of trajectory used for analysis). A 2 fs timestep was used, and atomic positions were stored during production at 1 ps intervals. Periodic boundary conditions were implemented, as well as SHAKE[60] with an accuracy tolerance of 10^{-4} to constrain hydrogen−carbon bond lengths. For all analyses, 10 ns production simulations were sampled every 100 ps. $g_{ij}(r)$ used for $S(q)$ calculations were calculated using a 0.1 Å bin width and an r_{max} of 22 Å. The simulations were systematically approximately 3% more dense than experiment at each temperature, consistent with others' findings for the CL&P force field.[54]

RESULTS AND DISCUSSION

Figure 1A shows the calculated total $S(q)$ for C_4C_1pyrrTFSI for q < 2.0 Å^{-1} at 298, 363, and 500 K (temperatures above its melting point and below its decomposition temperature). The figure verifies that peaks calculated near q = 0.795 and 1.25 Å^{-1} shift to lower q and increase in intensity as temperature increases (a comparison of calculated and experimentally

DOI: 10.1021/acs.jpcb.9b00449
J. Phys. Chem. B 2019, 123, 1672−1678

Table 2. Positive and Negative Components of $S(q)$ and Partial $S(q)$ at q = 1.25 Å^{-1} [a]

	298 K	500 K	difference	percent of difference
$S(q)$	1.27	1.74	0.46	100.00
positive contribution	7.73	7.18	−0.55	−119.09
negative contribution	−6.46	−5.44	1.02	219.09
positive contribution cation−cation	1.18	1.08	−0.11	−23.35
negative contribution cation−cation	−0.71	−0.63	0.07	15.75
positive contribution anion−anion	3.38	3.13	−0.25	−53.83
negative contribution anion−anion	−3.19	−2.80	0.39	84.42
positive contribution cation−anion	3.16	2.97	−0.19	−41.92
negative contribution cation−anion	−2.56	−2.01	0.55	118.92

[a]Positive and negative contributions to $S(q)$ (rows 2 and 3) each indicate structural ordering and sum to $S(q)$ (row 1). Positive and negative contributions to partial $S(q)$ (rows 4−9) also sum to $S(q)$ (row 1). For increasing temperature (298 to 500 K), the negative contribution decreases in magnitude more than the positive contribution, which causes $S(q)$ to increase in magnitude with increasing temperature. Numbers are rounded to two decimal places.

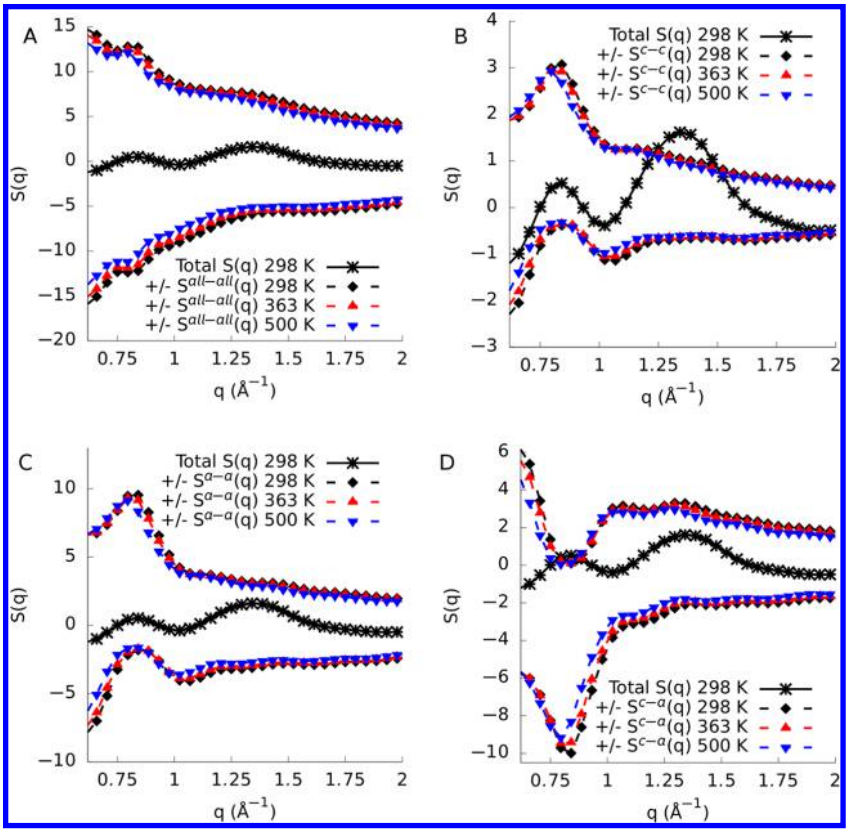

Figure 3. (A) Temperature trends for positive and negative components of static structure factor ($S(q)$) shown with $S(q)$ at 298 K. Positive and negative components each indicate structural ordering. The two dashed black diamond curves sum to $S(q)$ (i.e., total $S(q)$) at 298 K. Temperature trends for positive and negative components of (B) cation−cation partial $S(q)$, (C) anion−anion $S(q)$, and (D) cation−anion, each shown alongside total $S(q)$ at 298 K. The six dashed black diamond curves (two each in B, C, and D) sum to $S(q)$ at 298 K. Positive components at each q are in phase with each other, as are negative components, irrespective of whether $S(q)$ or partial $S(q)$ are positive or negative.

measured $S(q)$ for a larger range of q at 298 K is shown in the Supporting Information). Parts B, C, and D of Figure 1 show cation−cation, anion−anion, and cation−anion partial $S(q)$, respectively, calculated at the same temperatures.

Inspection of Fourier transform summands shows that the total $S(q)$ (Figure 2A) and each partial $S(q)$ (not shown) are composed of positive and negative contributions. Positive $S(q)$ contributions correspond to the positive summands from eq 1, whereas negative contributions correspond to the negative summands. The Fourier transform summands indicate the magnitude of the positive or negative contribution of each $g_{ij}(r)$ bin to $S(q)$ at one value of q (e.g., q = 0.795 Å^{-1} for Figure 2A). Figure 2B shows the difference in Fourier transform summands at q = 0.795 Å^{-1} for 500 K minus those for 298 K. Blue and red coloring is used to indicate where in r the 298 K contributions were positive and negative, respectively. Bars above the horizontal axis indicate that contributions become more positive (less negative) at 500 K, and bars below the axis indicate that contributions become less positive (more negative) at 500 K. Thus, red bars above the horizontal axis indicate negative contributions to $S(q)$ at 298 K that become more positive (less negative) at 500 K. Thus, Figure 2B shows that the largest changes to $S(q)$ occur because negative contributions at 298 K, most evident between

DOI: 10.1021/acs.jpcb.9b00449
J. Phys. Chem. B 2019, 123, 1672−1678

approximately 1 and 3 Å (and to a lesser extent, from 5 to 15 Å), become less negative at 500 K. Plots such as those in Figure 2 can be made for any partial $S(q)$.

Table 1 shows numbers that may be generated using plots such as those in Figure 2, grouped to highlight subsets of atom types associated with the atomic distances used to calculate $g_{ij}(r)$. The table also shows the difference between $S(q)$ at two temperatures (298 and 500 K) and the percentage of that difference represented by the positive and negative components. First, it is important to emphasize that each partial $S(q)$, whether positive or negative at any given q, is composed of both positive and negative components. Second, the dominant contributions to peak 1 $S(q)$ at q = 0.795 Å^{-1} at 298 K (Table 1) are −9.71 from cation−anion and +9.46 from anion−anion. The total contribution (that is to say, positive contribution plus magnitude of negative contribution) of anion−anion is 11.63, that of cation−cation is 3.47, and that of cation−anion is 10.03. Therefore, the peak is predominantly charge alternation (15.1 combined contribution from anion−anion and cation−cation contributions) and nontrivially cation−anion (total contribution of 10.03). Because the contributions are form factor weighted and most anion atoms have larger form factor weights than cation atoms, it is not surprising that anion−anion is the dominant contributor. Next, the difference in magnitude of the negative contributions to $S(q)$ at the two temperatures is nearly twice that of the positive contribution (+1.18 vs −0.64). Finally, the largest changes in magnitude appear in the negative contributions from cation−anion (101.7%) and anion−anion (90.6%) distances. The dominant contributions to peak 2 $S(q)$ at q = 1.25 Å^{-1} at 298 K (Table 2) are +3.38 and −3.19 from anion−anion distances (for a total contribution of 6.57) and +3.16 and −2.56 from cation−anion distances (for a total contribution of 5.72), so the peak is primarily composed of anion−anion and cation−anion contributions. The cation−cation contributions are +1.18 and −0.71 (for a total magnitude of 1.89). Again, anion atoms generally have the largest form factor weights, a significant influence in making them the largest contribution to $S(q)$. When the temperature increases, the negative (phase-shifted) contributions to $S(q)$ again decrease in magnitude more than the positive contributions decrease (+1.02 vs −0.55). Thus, for both the peak centered near q = 0.795 Å^{-1} and 1.25 Å^{-1}, peak heights grow upon heating from 298 to 500 K because the negative, phase-shifted contributions to $S(q)$ and partial $S(q)$ decrease in magnitude more than the positive contributions decrease (Figure 3). Therefore, we conclude that the structural ordering in C_4C_1pyrrTFSI responsible for the observed peaks centered near q = 0.795 and 1.25 Å^{-1} in total $S(q)$ decohere with increasing temperature even though those peaks show increasing intensity with increasing temperature. Figure 3 shows that these findings are not specific to q = 0.795 and 1.25 Å^{-1} but also hold for q values near q = 0.795 and 1.25 Å^{-1}.

CONCLUSIONS

In summary, this work proposes decomposing discrete Fourier transforms into component summands, analyzes Fourier transform summands for total and partial $S(q)$ calculated from MD simulations, and illustrates their utility by examining the temperature-dependent intensity increase observed for low-q peaks in $S(q)$ for C_4C_1pyrrTFSI. First, our analysis confirms that the peak calculated to appear near q = 0.795 Å^{-1}, peak 1, arises mostly from charge alternation (distances between like charges, primarily anion−anion distances). The peak near q = 1.25 Å^{-1}, peak 2, is due primarily to cation−anion and anion−anion distances. That anions are significant contributors to both peak 1 and peak 2 is due in part to the greater form factor weights associated with most anion atoms than cation atoms. Second, $S(q)$ and partial $S(q)$ calculated from MD simulations are decomposed into positive and negative components by separately summing the positive and negative Fourier transform summands before adding them to give partial or total $S(q)$. Positive and negative components of partial and total $S(q)$ are of the same ordering type (e.g., cation−anion) and have the same periodicity at a given q, but they are offset by a real space phase shift. C_4C_1pyrrTFSI's two low-q $S(q)$ peaks increase in intensity with increasing temperature because the sum of the negative components of the partial $S(q)$ decreases in magnitude more than the sum of the positive components does. Thus, the structuring in C_4C_1pyrrTFSI with periodicities corresponding to observed $S(q)$ peaks centered near q = 0.795 and 1.25 Å^{-1} decoheres, even though those peaks in $S(q)$ show increasing intensity with increasing temperature. This argues for great caution when interpreting $S(q)$ intensities and highlights the value of simulations (e.g., MD or Monte Carlo simulations) as a complement to X-ray (or neutron) scattering experiments.

While this study focuses on $S(q)$ and three partial $S(q)$ (cation−cation, anion−anion, and cation−anion), the atoms can be grouped in any other way (e.g., cation−cation decomposed into ring−tail, ring−ring, and tail−tail). Because we envision more general uses for the Fourier transform summand decomposition to interpret $S(q)$ for any type of soft matter, two of us (T.M. and R.A.W.) are preparing an open source VMD[61] module, *viewSq*. The module will allow users to quantify the contribution of each atomic or group pair to $S(q)$ with or without form factor weights, use the Fourier transform summands to rank atoms or groups of atoms by their contributions to each q, and thereby visualize the atoms or groups of atoms making the largest contribution(s) to $S(q)$.

ASSOCIATED CONTENT

Supporting Information

The Supporting Information is available free of charge on the ACS Publications website at DOI: 10.1021/acs.jpcb.9b00449.

Comparison of calculated and experimental $S(q)$; Fourier transform summands and their differences at two temperatures for q = 1.25 Å^{-1} (PDF)

AUTHOR INFORMATION

Corresponding Author

*E-mail: rwheeler5@niu.edu.

ORCID

Travis Mackoy: 0000-0003-3596-0223

Ralph A. Wheeler: 0000-0002-4158-823X

Notes

The authors declare no competing financial interest.

ACKNOWLEDGMENTS

We thank and acknowledge Bharat Kale from Professor Michael Papka's research group in the Department of Computer Science at Northern Illinois University for discussions and for his work writing computer code for *viewSq*. We also thank and acknowledge Reese Richardson for

DOI: 10.1021/acs.jpcb.9b00449
J. Phys. Chem. B 2019, 123, 1672−1678

discussions regarding projects related to the work presented here. Computer resources used for molecular dynamics simulations were provided in part by the Center for Research Computing and Data at Northern Illinois University. This work also used resources funded by National Science Foundation grants CHE-0321147, CHE-0723109, and CHE-1126465. T.M.'s salary was provided by a research assistantship funded by Northern Illinois University. The National Science Foundation (NSF) Research Experience for Undergraduates (REU) grant CHE-1659548 provided funding for collaboration between coauthors.

REFERENCES

(1) Welton, T. Room-Temperature Ionic Liquids. Solvents for Synthesis and Catalysis. *Chem. Rev.* **1999**, *99*, 2071−2083.
(2) Rogers, R. D.; Seddon, K. R. Ionic Liquids–Solvents of the Future? *Science* **2003**, *302*, 792−793.
(3) Kubisa, P. Application of Ionic Liquids as Solvents for Polymerization Processes. *Prog. Polym. Sci.* **2004**, *29*, 3−12.
(4) Peng, J.; Deng, Y. Cycloaddition of Carbon Dioxide to Propylene Oxide Catalyzed by Ionic Liquids. *New J. Chem.* **2001**, *25*, 639−641.
(5) Sheldon, R. A. Catalytic Reactions in Ionic Liquids. *Chem. Commun.* **2001**, *23*, 2399−2407.
(6) Khani, H.; Rofouei, M. K.; Arab, P.; Gupta, V. K.; Vafaei, Z. Multi-Walled Carbon Nanotubes-Ionic Liquid-Carbon Paste Electrode as a Super Selectivity Sensor: Application to Potentiometric Monitoring of Mercury Ion (II). *J. Hazard. Mater.* **2010**, *183*, 402−409.
(7) *Electrochemical Aspects of Ionic Liquids*, 2nd ed.; Ohno, H., Ed.; John Wiley & Sons: Hoboken, NJ, 2011.
(8) Freemantle, M. *An Introduction to Ionic Liquids*; The Royal Society of Chemistry: Cambridge, U.K., 2010.
(9) Hayes, R.; Warr, G. G.; Atkin, R. Structure and Nanostructure in Ionic Liquids. *Chem. Rev.* **2015**, *115*, 6357−6426.
(10) Armand, M.; Endres, F.; MacFarlane, D. R.; Ohno, H.; Scrosati, B. Ionic-Liquid Materials for the Electrochemical Challenges of the Future. *Nat. Mater.* **2009**, *8*, 621−629.
(11) Murphy, T.; Atkin, R.; Warr, G. G. Scattering from Ionic Liquids. *Curr. Opin. Colloid Interface Sci.* **2015**, *20*, 282−292.
(12) Russina, O.; Triolo, A.; Gontrani, L.; Caminiti, R. Mesoscopic Structural Heterogeneities in Room-Temperature Ionic Liquids. *J. Phys. Chem. Lett.* **2012**, *3*, 27−33.
(13) *The Structure of Ionic Liquids*; Caminiti, R., Gontrani, L., Eds.; Springer: Heidelberg, Germany, 2014.
(14) Freitas, A. A.; Shimizu, K.; Lopes, J. N. C. Complex Structure of Ionic Liquids. Molecular Dynamics Studies with Different Cation−Anion Combinations. *J. Chem. Eng. Data* **2014**, *59*, 3120−3129.
(15) Triolo, A.; Russina, O.; Bleif, H. J.; Di Cola, E. Nanoscale Segregation in Room Temperature Ionic Liquids. *J. Phys. Chem. B* **2007**, *111*, 4641−4644.
(16) Shimizu, K.; Bernardes, C. E. S.; Lopes, J. N. C. Structure and Aggregation in the 1-Alkyl-3-Methylimidazolium Bis-(Trifluoromethylsulfonyl)Imide Ionic Liquid Homologous Series. *J. Phys. Chem. B* **2014**, *118*, 567−576.
(17) Edson, D.; Pueblo, C.; Blodgett, M. E.; Kelton, K. F.; Mauro, N. A. Anomalous Temperature Dependence in the Structural Organization of Charge Alternation in Imidazolium-Based Ionic Liquids of Various Alkyl Chain Lengths. *J. Mol. Liq.* **2017**, *242*, 807−811.
(18) Ji, Y.; Shi, R.; Wang, Y.; Saielli, G. Effect of the Chain Length on the Structure of Ionic Liquids: From Spatial Heterogeneity to Ionic Liquid Crystals. *J. Phys. Chem. B* **2013**, *117*, 1104−1109.
(19) Canongia Lopes, J. N.; Pádua, A. A. H. CL&P: A Generic and Systematic Force Field for Ionic Liquids Modeling. *Theor. Chem. Acc.* **2012**, *131*, 1−11.
(20) Siqueira, L. J. A.; Ribeiro, M. C. C. Charge Ordering and Intermediate Range Order in Ammonium Ionic Liquids. *J. Chem. Phys.* **2011**, *135*, 204506.
(21) Wang, Y.; Voth, G. A. Tail Aggregation and Domain Diffusion in Ionic Liquids. *J. Phys. Chem. B* **2006**, *110*, 18601−18608.
(22) Raju, S. G.; Hariharan, K. S.; Park, D.; Kang, H. Effects of Variation in Chain Length on Ternary Polymer Electrolyte - Ionic Liquid Mixture - A Molecular Dynamics Simulation Study. *J. Power Sources* **2015**, *293*, 983−992.
(23) Wang, Y.; Jiang, W.; Voth, G. A. Unique Spatial Heterogeneity in Ionic Liquids. *J. Am. Chem. Soc.* **2005**, *127*, 12192−12193.
(24) Santos, C. S.; Murthy, N. S.; Baker, G. A.; Castner, E. W. Communication: X-Ray Scattering from Ionic Liquids with Pyrrolidinium Cations. *J. Chem. Phys.* **2011**, *134*, 121101.
(25) Li, S.; Banuelos, J. L.; Jianchang, G.; Anovitz, L.; Rother, G.; Shaw, R. W.; Hillesheim, P. C.; Dai, S.; Baker, G. A.; Cummings, P. T. Alkyl Chain Length and Temperature Effects on Structural Properties of Pyrrolidinium-Based Ionic Liquids: A Combined Atomistic Simulation and Small-Angle X-Ray Scattering Study. *J. Phys. Chem. Lett.* **2012**, *3*, 125−130.
(26) Kashyap, H. K.; Hettige, J. J.; Annapureddy, H. V. R.; Margulis, C. J. SAXS Anti-Peaks Reveal the Length-Scales of Dual Positive-Negative and Polar-Apolar Ordering in Room-Temperature Ionic Liquids. *Chem. Commun.* **2012**, *48*, 5103−5105.
(27) Kashyap, H. K.; Santos, C. S.; Murthy, N. S.; Hettige, J. J.; Kerr, K.; Ramati, S.; Gwon, J.; Gohdo, M.; Lall-Ramnarine, S. I.; Wishart, J. F.; et al. Structure of 1-Alkyl-1-Methylpyrrolidinium Bis-(Trifluoromethylsulfonyl)Amide Ionic Liquids with Linear, Branched, and Cyclic Alkyl Groups. *J. Phys. Chem. B* **2013**, *117*, 15328−15337.
(28) Borodin, O.; Smith, G. D. Structure and Dynamics of N-Methyl-N-Propylpyrrolidinium Bis(Trifluoromethanesulfonyl)Imide Ionic Liquid from Molecular Dynamics Simulations. *J. Phys. Chem. B* **2006**, *110*, 11481−11490.
(29) Fujimori, T.; Fujii, K.; Kanzaki, R.; Chiba, K.; Yamamoto, H.; Umebayashi, Y.; Ishiguro, S. Conformational Structure of Room Temperature Ionic Liquid N-Butyl-N-Methyl-Pyrrolidinium Bis-(Trifluoromethanesulfonyl) Imide - Raman Spectroscopic Study and DFT Calculations. *J. Mol. Liq.* **2007**, *131−132*, 216−224.
(30) Fukuda, S.; Takeuchi, M.; Fujii, K.; Kanzaki, R.; Takamuku, T.; Chiba, K.; Yamamoto, H.; Umebayashi, Y.; Ishiguro, S. Liquid Structure of N-Butyl-N-Methylpyrrolidinium Bis-(Trifluoromethanesulfonyl)Amide Ionic Liquid Studied by Large Angle X-Ray Scattering and Molecular Dynamics Simulations. *J. Mol. Liq.* **2008**, *143*, 2−7.
(31) Funston, A. M.; Fadeeva, T. A.; Wishart, J. F.; Castner, E. W. Fluorescence Probing of Temperature-Dependent Dynamics and Friction in Ionic Liquid Local Environments. *J. Phys. Chem. B* **2007**, *111*, 4963−4977.
(32) Hayamizu, K.; Tsuzuki, S.; Seki, S.; Fujii, K.; Suenaga, M.; Umebayashi, Y. Studies on the Translational and Rotational Motions of Ionic Liquids Composed of N-Methyl-N-Propyl-Pyrrolidinium (P13) Cation and Bis(Trifluoromethanesulfonyl)Amide and Bis-(Fluorosulfonyl)Amide Anions and Their Binary Systems Including Lithium Salts. *J. Chem. Phys.* **2010**, *133*, 194505.
(33) Harris, K. R.; Woolf, L. A.; Kanakubo, M.; Rüther, T. Transport Properties of N-Butyl-N-Methylpyrrolidinium Bis-(Trifluoromethylsulfonyl)Amide. *J. Chem. Eng. Data* **2011**, *56*, 4672−4685.
(34) Haskins, J. B.; Bennett, W. R.; Wu, J. J.; Hernández, D. M.; Borodin, O.; Monk, J. D.; Bauschlicher, C. W.; Lawson, J. W. Computational and Experimental Investigation of Li-Doped Ionic Liquid Electrolytes: [Pyr14][TFSI], [Pyr13][FSI], and [EMIM]-[BF4]. *J. Phys. Chem. B* **2014**, *118*, 11295−11309.
(35) Henderson, W. A.; Young, V. G.; Passerini, S.; Trulove, P. C.; De Long, H. C.; Young, V. G. Plastic Phase Transitions in N-Ethyl-N-Methylpyrrolidinium Bis(Trifluoromethanesulfonyl)Imide. *Chem. Mater.* **2006**, *18*, 934−938.

DOI: 10.1021/acs.jpcb.9b00449
J. Phys. Chem. B 2019, 123, 1672−1678

(36) Kunze, M.; Jeong, S.; Paillard, E.; Winter, M.; Passerini, S. Melting Behavior of Pyrrolidinium-Based Ionic Liquids and Their Binary Mixtures. *J. Phys. Chem. C* **2010**, *114*, 12364−12369.
(37) Lahiri, A.; Carstens, T.; Atkin, R.; Borisenko, N.; Endres, F. In Situ Atomic Force Microscopic Studies of the Interfacial Multilayer Nanostructure of LiTFSI−[Py1, 4]TFSI on Au(111): Influence of Li + Ion Concentration on the Au(111)/IL Interface. *J. Phys. Chem. C* **2015**, *119*, 16734−16742.
(38) Lauw, Y.; Horne, M. D.; Rodopoulos, T.; Lockett, V.; Akgun, B.; Hamilton, W. A.; Nelson, A. R. Structure of [C4mpyr][NTf2] Room-Temperature Ionic Liquid at Charged Gold Interfaces. *Langmuir* **2012**, *28*, 7374−7381.
(39) Li, Z.; Borodin, O.; Smith, G. D.; Bedrov, D. Effect of Organic Solvents on Li+ Ion Solvation and Transport in Ionic Liquid Electrolytes: A Molecular Dynamics Simulation Study. *J. Phys. Chem. B* **2015**, *119*, 3085−3096.
(40) Canongia Lopes, J. N.; Shimizu, K.; Pádua, A. A. H.; Umebayashi, Y.; Fukuda, S.; Fujii, K.; Ishiguro, S. A Tale of Two Ions: The Conformational Landscapes of Bis-(Trifluoromethanesulfonyl)Amide and N,N-Dialkylpyrrolidinium. *J. Phys. Chem. B* **2008**, *112*, 1465−1472.
(41) Sharma, S.; Gupta, A.; Kashyap, H. K. How the Structure of Pyrrolidinium Ionic Liquids Is Susceptible to High Pressure. *J. Phys. Chem. B* **2016**, *120*, 3206−3214.
(42) Smith, A. M.; Lovelock, K. R. J.; Gosvami, N. N.; Licence, P.; Dolan, A.; Welton, T.; Perkin, S. Monolayer to Bilayer Structural Transition in Confined Pyrrolidinium-Based Ionic Liquids. *J. Phys. Chem. Lett.* **2013**, *4*, 378−382.
(43) Solano, C. J. F.; Jeremias, S.; Paillard, E.; Beljonne, D.; Lazzaroni, R. A Joint Theoretical/Experimental Study of the Structure, Dynamics, and Li+ Transport in Bis([Tri]Fluoro-[Methane]Sulfonyl)Imide [T]FSI-Based Ionic Liquids. *J. Chem. Phys.* **2013**, *139*, 034502.
(44) Umebayashi, Y.; Mitsugi, T.; Fujii, K.; Seki, S.; Chiba, K.; Yamamoto, H.; Lopes, J. N. C.; Pádua, A. A. H.; Takeuchi, M.; Kanzaki, R.; et al. Raman Spectroscopic Study, DFT Calculations and MD Simulations on the Conformational Isomerism of N-Alkyl-N-Methylpyrrolidinium Bis-(Trifluoromethanesulfonyl) Amide Ionic Liquids. *J. Phys. Chem. B* **2009**, *113*, 4338−4346.
(45) Umebayashi, Y.; Hamano, H.; Seki, S.; Minofar, B.; Fujii, K.; Hayamizu, K.; Tsuzuki, S.; Kameda, Y.; Kohara, S.; Watanabe, M. Liquid Structure of and Li+ Ion Solvation in Bis-(Trifluoromethanesulfonyl)Amide Based Ionic Liquids Composed of 1-Ethyl-3-Methylimidazolium and N-Methyl-N-Propylpyrrolidinium Cations. *J. Phys. Chem. B* **2011**, *115*, 12179−12191.
(46) Vicent-Luna, J. M.; Ortiz-Roldan, J. M.; Hamad, S.; Tena-Zaera, R.; Calero, S.; Anta, J. A. Quantum and Classical Molecular Dynamics of Ionic Liquid Electrolytes for Na/Li-Based Batteries: Molecular Origins of the Conductivity Behavior. *ChemPhysChem* **2016**, *17*, 2473−2481.
(47) Xu, C.; Durumeric, A.; Kashyap, H. K.; Kohanoff, J.; Margulis, C. J. Dynamics of Excess Electronic Charge in Aliphatic Ionic Liquids Containing the Bis(Trifluoromethylsulfonyl)Amide Anion. *J. Am. Chem. Soc.* **2013**, *135*, 17528−17536.
(48) Araque, J. C.; Hettige, J. J.; Margulis, C. J. Modern Room Temperature Ionic Liquids, a Simple Guide to Understanding Their Structure and How It May Relate to Dynamics. *J. Phys. Chem. B* **2015**, *119*, 12727−12740.
(49) Murad, S.; Evans, D. J.; Gubbins, K. E.; Streett, W. B.; Tildesley, D. J. Molecular Dynamics Simulation of Dense Fluid Methane. *Mol. Phys.* **1979**, *37*, 725−736.
(50) Santos, C. S.; Annapureddy, H. V. R.; Murthy, N. S.; Kashyap, H. K.; Castner, E. W.; Margulis, C. J. Temperature-Dependent Structure of Methyltributylammonium Bis(Trifluoromethylsulfonyl)-Amide: X Ray Scattering and Simulations. *J. Chem. Phys.* **2011**, *134*, 064501.
(51) Faber, T. E.; Ziman, J. M. A Theory of the Electrical Properties of Liquid Metals: III. The Resistivity of Binary Alloys. *Philos. Mag.* **1965**, *11*, 153−173.
(52) *International Tables for Crystallography*, Vol. C; Prince, E., Ed.; International Union of Crystallography: Chester, U.K., 2006.
(53) Plimpton, S. Fast Parallel Algorithms for Short − Range Molecular Dynamics. *J. Comput. Phys.* **1995**, *117*, 1−19.
(54) Canongia Lopes, J. N.; Deschamps, J.; Pádua, A. A. H. Modeling Ionic Liquids Using a Systematic All-Atom Force Field. *J. Phys. Chem. B* **2004**, *108*, 2038−2047.
(55) Rizzo, R. C.; Jorgensen, W. L. OPLS All-Atom Model for Amines: Resolution of the Amine Hydration Problem. *J. Am. Chem. Soc.* **1999**, *121*, 4827−4836.
(56) Hockney, R. W.; Eastwood, J. W. *Computer Simulation Using Particles*; Taylor & Francis Group: New York, 1988.
(57) Shinoda, W.; Shiga, M.; Mikami, M. Rapid Estimation of Elastic Constants by Molecular Dynamics Simulation under Constant Stress. *Phys. Rev. B: Condens. Matter Mater. Phys.* **2004**, *69*, 134103.
(58) Tuckerman, M. E.; Alejandre, J.; López-Rendón, R.; Jochim, A. L.; Martyna, G. J. A Liouville-Operator Derived Measure-Preserving Integrator for Molecular Dynamics Simulations in the Isothermal-Isobaric Ensemble. *J. Phys. A: Math. Gen.* **2006**, *39*, 5629.
(59) Martínez, L.; Andrade, R.; Birgin, E. G.; Martínez, J. M. Packmol: A Package for Building Initial Configurations for Molecular Dynamics Simulations. *J. Comput. Chem.* **2009**, *30*, 2157−2164.
(60) Ryckaert, J.-P.; Ciccotti, G.; Berendsen, H. J. C. Numerical Integration of the Cartesian Equations of Motion of a System with Constraints: Molecular Dynamics of n-Alkanes. *J. Comput. Phys.* **1977**, *23*, 327−341.
(61) Humphrey, W.; Dalke, A.; Schulten, K. VMD: Visual Molecular Dynamics. *J. Mol. Graphics* **1996**, *14*, 33−38.

DOI: 10.1021/acs.jpcb.9b00449
J. Phys. Chem. B 2019, 123, 1672−1678